PROCEEDINGS, 49th Workshop on Geothermal Reservoir Engineering
Stanford University, Stanford, California, February 12-14, 2024
SGP-TR-227

Deep Learning to Infer Geothermal Reservoir Quality from Scanning Electron Microscope (SEM) Images

Arkanu Andaru[1], Sarah Sausan[2]

[1]School of Computing, Australian National University

[2]Dept. of Energy Science and Engineering, Stanford University

andaru@alumni.anu.edu.au

sausan@stanford.edu

Keywords: U-net, CNN, quartz overgrowth, back-scattered electron, cathodoluminescence, electron microscope.

ABSTRACT

This paper presents an update on a dynamic segmentation algorithm for detecting quartz overgrowths in geothermal reservoirs using Scanning Electron Microscope (SEM) images. Previously, the Random Forest algorithm had been employed in the automated workflow for quartz overgrowth detection from SEM images. A 75% accuracy score was achieved from the model training, indicating a promising start. This model was found to differentiate successfully between detrital quartz grains and their diagenetic quartz overgrowths; it was also demonstrated that it could identify porosity and other minerals.

A continuation of the algorithm development in the automated workflow is explored in this paper. Deep learning methods using U-net architecture is investigated to find the most fitting algorithm for detecting quartz overgrowth. The previously utilized texture-based feature extraction techniques are still incorporated. Normalization and dynamic overlaying algorithms are applied to address variations in image brightness and contrast and align BSE and CL images accurately, ensuring reliable segmentation. The segmentation process involves the coordination of BSE and CL images, utilizing their respective strengths, and overlaying them to achieve comprehensive results. This is followed by a two-fold model-building approach using separate segmentation models for BSE and CL images, which are then combined to distinguish between pore space, quartz grain, and quartz overgrowth.

The evaluation of the U-Net model's performance involves analysis of training and validation accuracy, loss, and intersection over union (IoU) over 50 epochs. Results demonstrate the model's capability to generalize and learn effectively, with the segmentation process showing proficiency in differentiating between the target mineralogy features. However, variability in performance across different datasets suggests the need for further model optimization.

In conclusion, the integration of U-Net into SEM image analysis for mineralogy detection represents a significant technological advance in geoscience, offering a more efficient, precise, and automated approach to understanding and exploiting geothermal energy resources. The findings also highlight opportunities for future research, such as exploring a variety of deep learning models, fine-tuning through transfer learning, and developing user-friendly tools for rapid mineralogy segmentation.

1. INTRODUCTION

The study of geothermal reservoirs is crucial for understanding and utilizing Earth's geothermal energy resources. In sedimentary geothermal reservoirs, permeability is a crucial property as it affects the flow rate of fluids through the reservoir, ultimately affecting the amount of energy that can be extracted. However, lower permeability than expected is a common problem in sedimentary geothermal reservoirs (Dillinger, et al., 2016), which can be caused by quartz overgrowth.

Quartz overgrowth, also referred to as quartz cement, emerges as a predominant diagenetic phase within sandstone formations. As the most abundant cement in sandstones, it significantly contributes to the overall diagenetic modification of these formations (Goldstein & Rossi, 2022). The process, involving the precipitation of quartz between sand grains, is known to markedly diminish the permeability in sedimentary geothermal reservoirs. Accurately identifying quartz overgrowths, therefore, is not just a matter of mineralogical interest but is instrumental in elucidating the diagenetic history and reservoir properties of sandstones. Traditional detection methods, primarily through Scanning Electron Microscope (SEM) analysis, however, present challenges in accuracy and efficiency, signaling the need for more advanced and reliable identification techniques.

Currently, one of the most common methods for analyzing quartz overgrowth in sedimentary geothermal reservoirs is through the use of Scanning Electron Microscopy (SEM) images. In the case of analyzing quartz overgrowth, two type of SEM images are used, Cathodoluminescence (CL) and Backscattered Electron (BSE). Analysis is typically done by manually examining thousands of BSE and CL images to identify the presence of quartz overgrowth based on their characteristic shape, size, and composition. The manual examination can be time-consuming and labor-intensive, especially when dealing with large numbers of images. Additionally, manual examination can be subject to human error, which can introduce inaccuracies in the analysis.

Presently, SEM images, particularly Cathodoluminescence (CL) and Backscattered Electron (BSE) modalities, are the cornerstone of quartz overgrowth analysis in sedimentary geothermal reservoirs. Typically, this involves a meticulous, manual examination of thousands of BSE and CL images, identifying quartz overgrowth based on distinct morphological characteristics such as shape, size, and composition. This manual process is not only time-intensive and laborious but is also prone to human error, potentially leading to inaccuracies in the analysis.

This paper seeks to present a comprehensive review of the current state of research on quartz overgrowths, while also highlighting recent advancements in identification techniques using deep learning. Special emphasis is placed on the relevance and applicability of these advancements in the context of sedimentary geothermal reservoirs. The objective is to underscore the significance of these developments in enhancing our understanding and exploitation of geothermal energy resources.

2. PREVIOUS WORK AND INITIAL FINDINGS

In our previous work (Andaru and Sausan, 2023), we developed an automated workflow using computer vision and machine learning techniques to detect diagenetic quartz overgrowths in sedimentary geothermal reservoirs. The automated workflow utilized a dynamic segmentation algorithm for detecting diagenetic quartz overgrowths in geothermal reservoirs. The algorithm, capable of handling SEM images with varying qualities, is enhanced with noise suppression and multi-level auto-thresholding. Trained using Random Forest on features like Gabor, Canny Edge, and Roberts Edge, the model achieves a 75% accuracy rate (Andaru and Sausan, 2023).

3. DEEP LEARNING IN AUTOMATED MINERAL IDENTIFICATION

The field of geoscience is currently undergoing a significant transformation through the integration of machine learning (ML) and deep learning (DL) technologies. In particular, these advanced computational techniques are proving to be highly valuable in mineral identification from thin sections of rock samples. The traditional approach to mineral identification has been a manual and time-consuming process, reliant on expert knowledge and subjective interpretation. The introduction of ML and DL offers a new horizon in precision, efficiency, and accuracy for this crucial aspect of geoscience.

DL techniques have been extensively studied in geoscience for petrophysical analysis in digital rock analysis. This analysis involves examining a range of rock samples, including cores, mineral grains (Latif et al., 2022; Maitre et al., 2019), hand-samples (Liu et al., 2023), petrographic thin sections (Su et al., 2020; Tang et al., 2023), and scanning electron microscopy (SEM) images. Among these, SEM images have received significant research attention, with several studies leveraging DL approaches to infer physical properties of different rock types for diverse applications. Consequently, there is a growing interest in using DL techniques to advance digital rock analysis and improve the accuracy of petrophysical analysis for various types of rocks.

For shale rock types, Bihani et al. (2022) employed a DL-based method for filtering and segmentation to identify pore and grain features from grayscale mudrock SEM images. Other researchers, such as Misra et al. (2019), have also utilized SEM images in the same type of rock to infer the composition of organic-rich shale, including pore, kerogen, matrix, and pyrite. Additionally, image segmentation has been applied to infer microstructures in shale from SEM images (Knaup et al., 2020; Tian & Daigle, 2019). DL has also been used by several researchers to infer rock properties from thin sections, such as petrographic thin sections or SEM images. For instance, Bihani et al. (2022) utilized a DL-based method for filtering and segmentation to identify pore and grain features from grayscale mudrock SEM images, while other researchers have employed segmentation in different rock image types to aid petrophysical analysis, such as sandstone SEM images.

Overall, it is evident that the integration of ML and DL has revolutionized the field of geoscience, particularly in mineral identification and petrophysical analysis of rock samples. The continued exploration and application of these advanced computational techniques hold great potential for advancing our understanding of the Earth's geological properties and processes.

4. DATA

4.1 Dataset

The original dataset, provided by The Geological Survey of Denmark and Greenland (GEUS), is a comprehensive collection that includes four sets of Scanning Electron Microscopy (SEM) images. These sets encompass Cathodoluminescence (CL), Back-Scattered Electrons (BSE), and Mineral Maps (MM), along with a labeled JSON file comprising 30 pixels from 200 CL images, which serves as the ground truth data. This dataset is publicly accessible at https://doi.org/10.22008/FK2/5TWAZK. Each dataset set represents a unique sample and comprises a suite of SEM images. These images feature a cathodoluminescence image, a back-scattered electrons contrast image, and a false-colored mineral map of each analyzed area. This diverse array of datasets provides a robust foundation for detailed geological analysis and research.

4.2 Scanning Microscope Electron (SEM) Images

To thoroughly comprehend the characteristics of geothermal reservoirs, we employ two distinct Scanning Electron Microscope (SEM) imaging modes – SEM-BSE (Backscattered Electron) and SEM-CL (Cathodoluminescence). SEM-BSE images offer insights into the elemental composition of the sample, with the contrast driven by the backscattered electrons collected by the detector. This mode differentiates quartz, usually shown in grey, from the pore space, typically depicted in black. Conversely, SEM-CL images convey information about the surface topography and composition of the materials, the contrast of which relies on the secondary electrons emitted from the sample. For our research purposes, SEM-CL is used to distinguish quartz overgrowths from the primary quartz.

By overlaying SEM-CL and SEM-BSE images, we gain a comprehensive understanding of the sedimentary geothermal reservoirs' microstructure. This combined view allows us to differentiate between various minerals present in the reservoir and scrutinize the distribution of quartz overgrowths, which significantly impact reservoir permeability. Ultimately, our objective is to establish an automated workflow that uses computer vision and machine learning algorithms for the analysis of quartz overgrowths in SEM images.

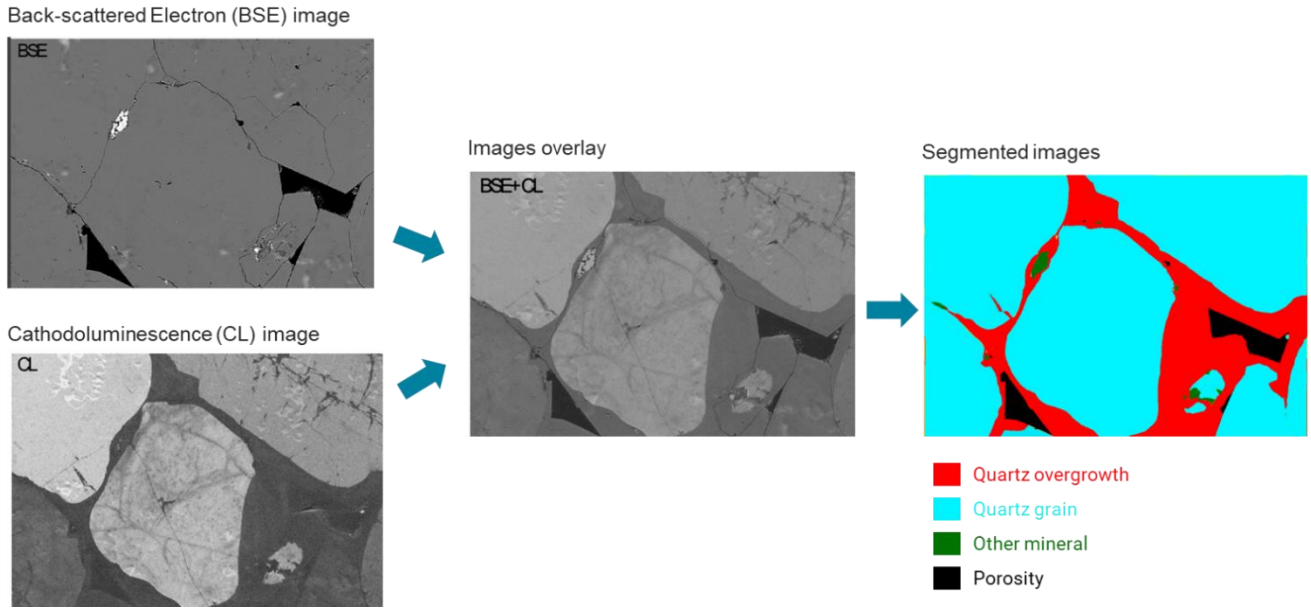

Figure 1: Illustration of mineral segmentation workflow using BSE and CL images.

4.2 Training Dataset

The labeled dataset for the training set, as established in our previous work (Andaru & Sausan, 2023), is derived from a 30-pixel labeled JSON of 200 CL images included in the dataset. Building upon this foundation, a full-image labeled dataset was created. This expansion involved geologist interpretation to extend the initially 30-pixel labeled data within each image. The extended labeled data is considered the Y parameter in the training dataset. Meanwhile, the X parameter is sourced from both the CL and BSE images in the dataset that have been labeled. For experimental purposes, we also combined and overlaid the CL and BSE images to serve as input parameters. The results and differences observed from this approach will be discussed in the subsequent 'Results and Discussion' section.

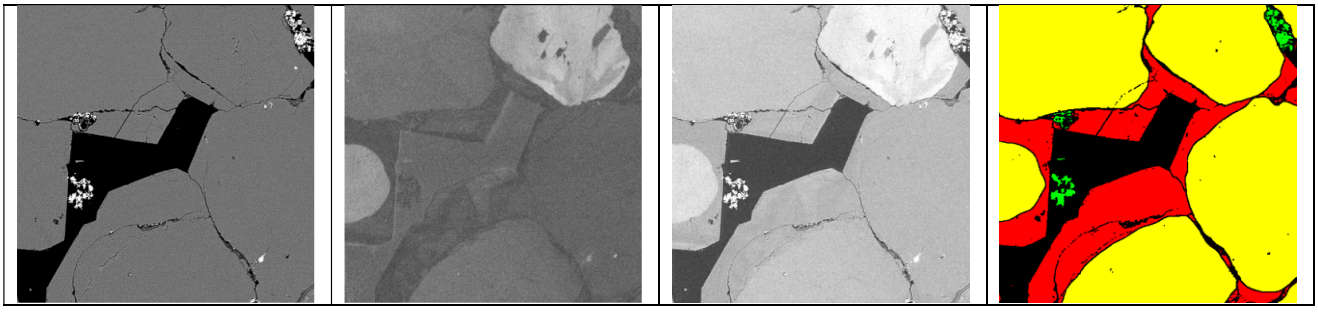

Figure 2: An example training data set, shown in four images from left to right: BSE, CL, BSE and CL overlaid and labeled, and BSE and CL overlaid.

5. METHOD

This study is focused on detecting four mineral categories using BSE and CL images. These categories are pore space, quartz grain, quartz overgrowth, and other minerals. Each BSE and CL image contains color and texture information that is represented through pixel value and spatial arrangement, which in turn represents each mineral category. However, BSE and CL have their own strengths in detecting minerals that we want to classify. For example, BSE images serve the best purpose in detecting pore space, quartz (which is a combination of quartz grain and its overgrowth), and other minerals. On the other hand, CL is best at detecting quartz grain. Therefore, our approach is to utilize both images to their strengths and then combine them for the final segmentation. The general workflow can be seen in Fig. 6.

5.1 Data Cleaning and Preparation

To accurately analyze mineralogy in Scanning Electron Microscope (SEM) images, a robust image processing workflow is necessary. First, the SEM images are normalized, then a dynamic overlaying algorithm is used to segment pore sp, quartz, quartz overgrowth, and other minerals. This algorithm combines SEM-CL and SEM-BSE images to achieve more precise segmentation. To compensate for any lateral or horizontal shifting present in some image pairs, the algorithm inputs the required shifting values for precise overlay alignment. The result is a comprehensive image processing workflow that ensures more precise and reliable mineralogy analysis.

Normalization

Normalization is a crucial step in ensuring consistency and reliability in image analysis. It involves adjusting the pixel values in images to a common scale, without distorting the differences in the ranges of values. This helps reduce variations caused by different brightness and contrast levels in datasets and individual image files, ensuring that machine learning models are not biased or misled by discrepancies in lighting or contrast. The process involves scaling the intensity values of each image to a standard range, usually between 0 and 1 or -1 and 1, resulting in a uniform appearance in terms of brightness and contrast. This allows the model to focus on the actual structural and compositional features of the samples, leading to more accurate and reliable outcomes in the analysis of SEM images.

Dynamic Overlaying

After implementing multi-level Otsu thresholding on both SEM-CL and SEM-BSE images, these images are merged to create a more detailed segmentation. This enhanced segmentation effectively differentiates between pore space, quartz, quartz overgrowth, and other mineral types. However, in some pairs of BSE and CL images, a misalignment is often noted, typically manifesting as a lateral or horizontal shift ranging from 5 to 10%. To address this issue, an algorithm has been developed specifically to accurately overlay SEM-BSE and SEM-CL images. This involves adjusting lateral and horizontal shifts for each image pair, as depicted in Figure 1. The effectiveness of this process is then verified through a manual review of 30-pixel labeled JSON data extracted from 200 CL images, enabling the generation of comprehensive ground truth data for the entire image.

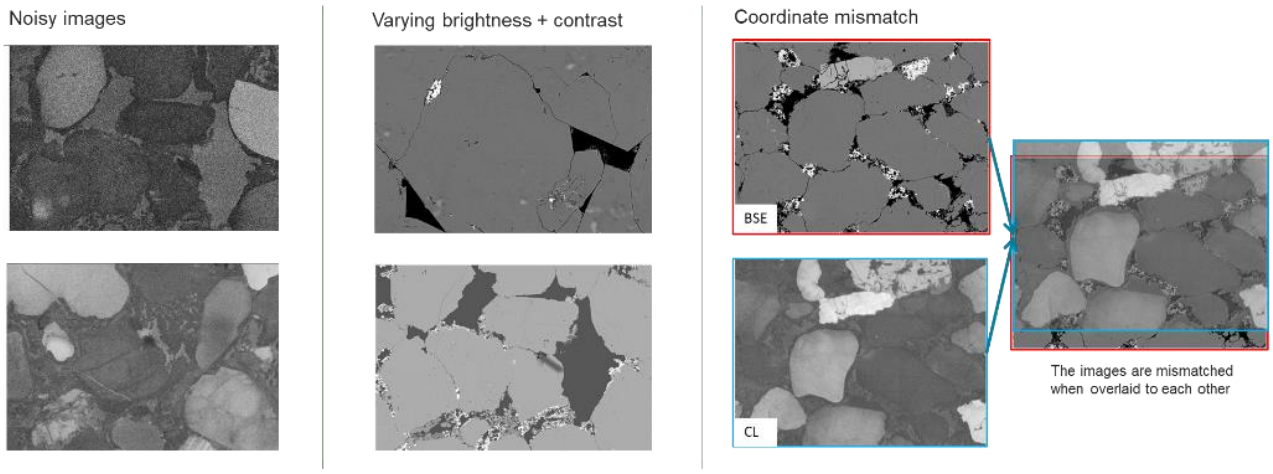

Figure 3: An instance of data inconsistency and misaligned coordinates within the provided dataset.

5.2 Image Slicing

Matching coordinates between Back-Scattered Electrons (BSE) and Cathodoluminescence (CL) images is a crucial aspect of this study. Overlaying these images is necessary to achieve the desired results. Although BSE and CL images do not align perfectly when overlaid, the labeled images match precisely with the BSE images. Therefore, during the data preprocessing stage, inputs from BSE, CL, and labeled images are sliced carefully to focus on the areas where BSE and CL intersect. This process is illustrated in **Error! Reference source not found.**, where the grey areas represent the intersected portions of BSE and CL in each image file.

To extract the intersected data, both images are sliced after determining the vertical and horizontal shift values for each dataset. Subsequently, the intersected segments of each BSE, CL, and labeled image are divided into two sections, each measuring 512 x 512 pixels (Figure 4). These segmented images are then utilized as the final images in the training dataset, ensuring that the data used for training is precisely aligned and representative of the intersected areas. This approach enhances the accuracy and relevance of the training dataset for the study.

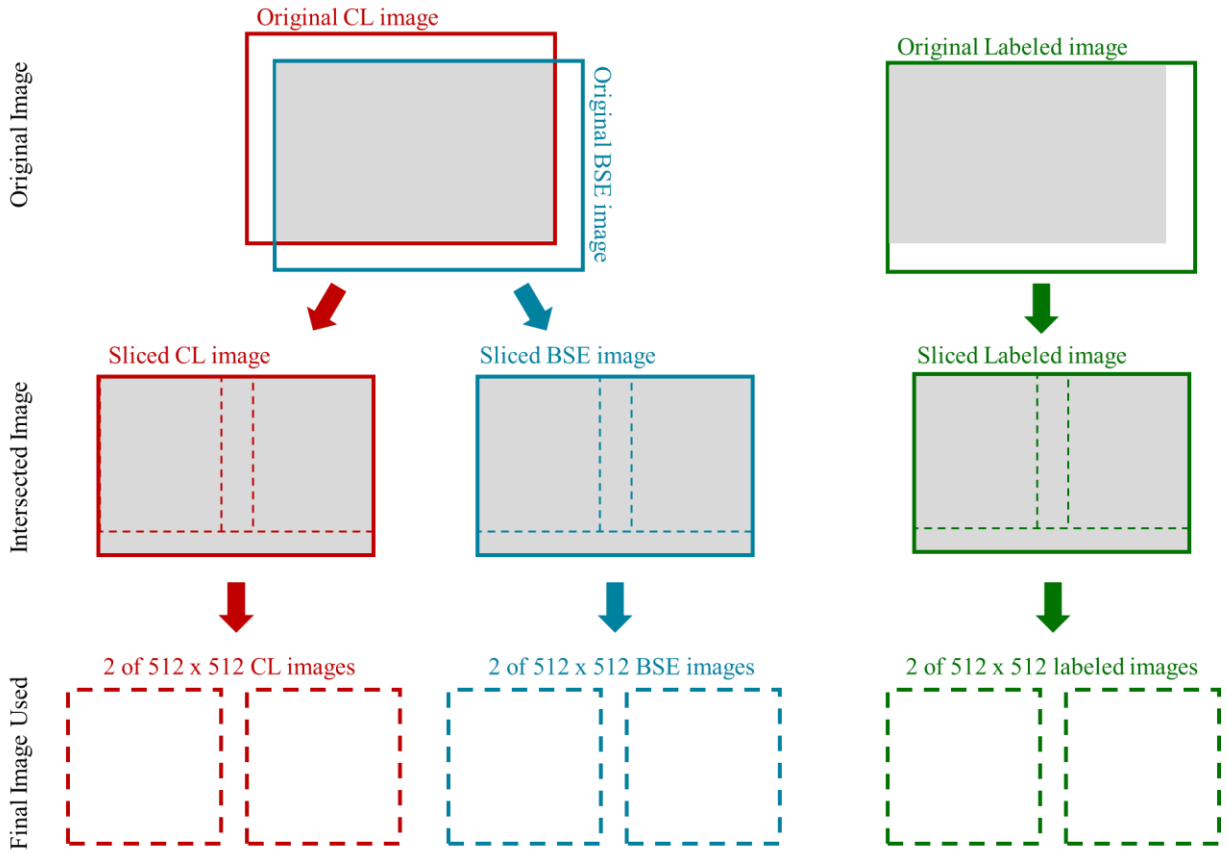

Figure 4: An illustration of the preparation process of slicing an image before it can be used

5.3 Model Building (U-Net)

The convolutional network is experimented in detecting mineralogy from BSE and CL images where classification is non-binary. In this case, multi-class label are expected to be determined from those BSE and CL images, pore space, quartz overgrowth and quartz grain. We utilized the network developed by Ronneberger et al. (2015) with modification catered to our purpose in detecting mineralogy via SEM images.

U-Net Architecture

In the geoscience research, particularly in the study of mineralogy through Scanning Electron Microscopy (SEM) images, the adoption of U-Net—a sophisticated convolutional neural network—marks a significant shift toward advanced computational methodologies. This paper explores the intricacies of U-Net's architecture and its substantial impact on improving the accuracy and efficiency of mineral detection and analysis in SEM imagery. U-Net's core design features a unique 'U'-shaped architecture that expertly balances the capture of contextual information with the precision of localization. This design consists of two main components: the contraction path and the expansive path. The contraction path, consists of repeated applications of convolutions followed by max pooling. This path is responsible for capturing the context in the image, which helps the network learn relevant features from the image that can determine pore space, quartz grain and quartz overgrowth. Conversely, the expansive path employs up-convolutional layers to progressively restore spatial resolution, enabling precise localization and delineation of mineralogy features within SEM images.

The contraction path is a technique of identifying quartz overgrowth from BSE and CL images. It is defined using a parameter that serves the purpose of the identification. The contraction path consists of applying 3x3 padded convolutions to maintain the same image output dimension as the input image. This is followed by a rectified linear unit (ReLU) and a 2x2 max pooling operation for each down-sampling repetition. In each repetition, the dimension is reduced by half. The expansive path is comprised of an up-sampling of the feature map followed by a 2x2 convolution that halves the number of feature channels. A concatenation with the corresponding feature map from the contracting path, and two 3x3 convolutions. In this U-net architecture, the input image size is 512x512 pixels and is down-sampled until 32x32 pixels through 4-step down-sampling. Later, it is up-sampled back to 512x512 pixels in the output image (Figure 5).

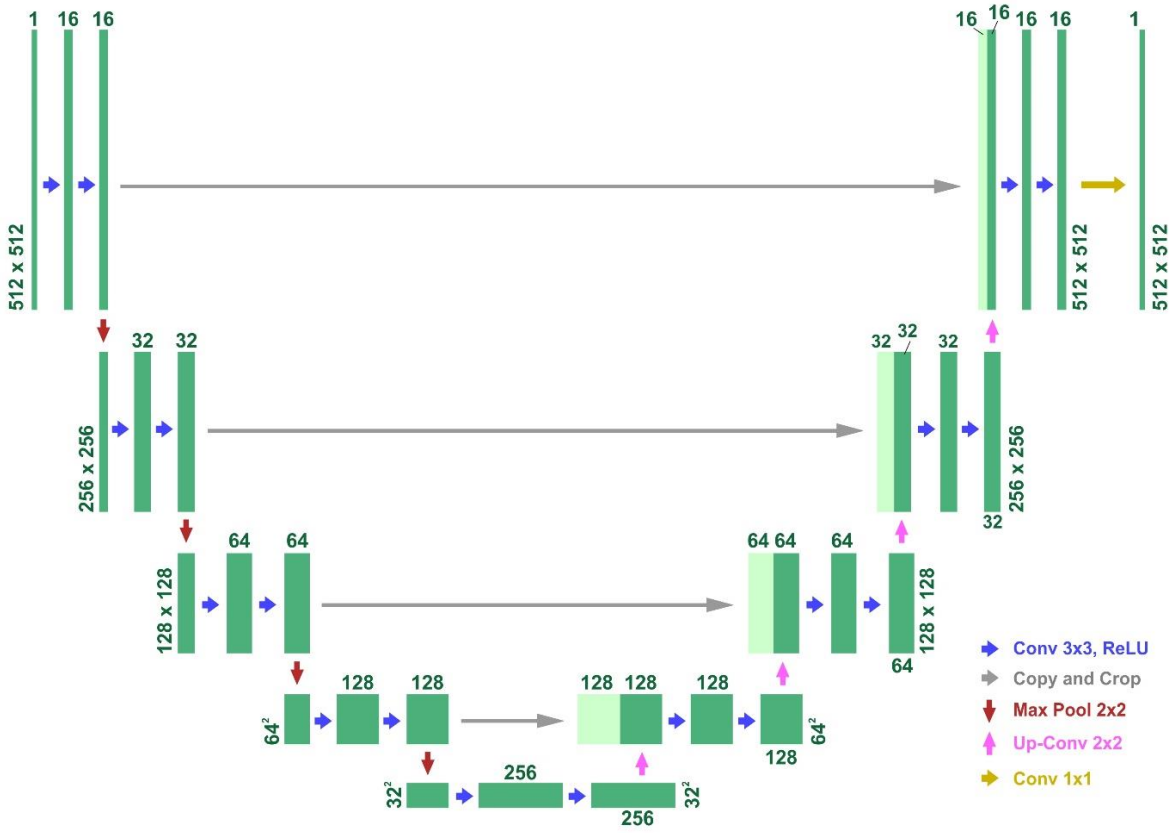

Figure 5: U-net architecture with a minimum resolution of 32x32 pixels. The green box represents a multi-channel feature map. The number on top of the box indicates the number of channels, and the number on the side of the box represents the x-y dimension.

Training Process

During the model training process, we tested two methods: using combined BSE and CL images as input, and building separate models for BSE and CL, which would later have their respective segmentation results overlaid in the finishing process. Our findings revealed that the latter method was more effective in detecting quartz growth identification. For the purposes of this paper, we utilized 18 combined BSE and CL images for the first method and 18 images of each BSE and CL image for the second approach.

To create the model, we developed separate segmentation models for BSE and CL due to their respective strengths in segmenting certain mineralogy features. BSE is most effective in segmenting pore space, other minerals, and quartz (both overgrowth and grain). However, BSE cannot differentiate between overgrowth and primary grain quartz. To address this, we built and trained a CL segmentation model to segment quartz grain and non-quartz grain. The CL image can distinguish primary quartz grain from its overgrowth, but it is less successful in detecting porosity. In some cases, porosity displays the same pixel intensity as quartz overgrowth, but quartz grain always has the highest pixel intensity. Therefore, we trained the CL segmentation to distinguish between quartz grain and non-quartz grain classes.

Thus, by combining both segmentation models, we can overlay the BSE and CL segmentation results to produce a final segmentation image that distinguishes all classes necessary for this paper: 1) pore space, 2) quartz grain, and 3) quartz overgrowth (Figure 6).

5.4 Mineralogy Prediction Workflow

Presented here is a workflow that showcases how mineral composition (Fig. 6), specifically pore space, quartz grain, and quartz overgrowth, can be predicted. See Fig. 6 for a visual representation. To begin, separate models are constructed for BSE and CL segmentation. These models are then utilized to predict new samples and calculate the composition of pore space, quartz grain, and quartz overgrowth in a set of BSE and CL images. To predict the composition, the BSE image is used as input and predicted utilizing the established model to obtain pore space and quartz (both grain and overgrowth quartz). Next, the CL data input is superimposed by the pore space obtained from BSE segmentation from the previous process. Then the overlaid CL is used as input to be predicted using the CL established model. The outcome will determine a segmentation of quartz grain. Finally, the result of the BSE, which displays a good delineation of quartz (grain and overgrowth) and pore space, and the CL, which displays a delineation of quartz grain, are overlaid to achieve the final segmentation. As a result, the percentage of mineral composition can be calculated from the final segmentation image to determine the number of percentages in each composition classification.

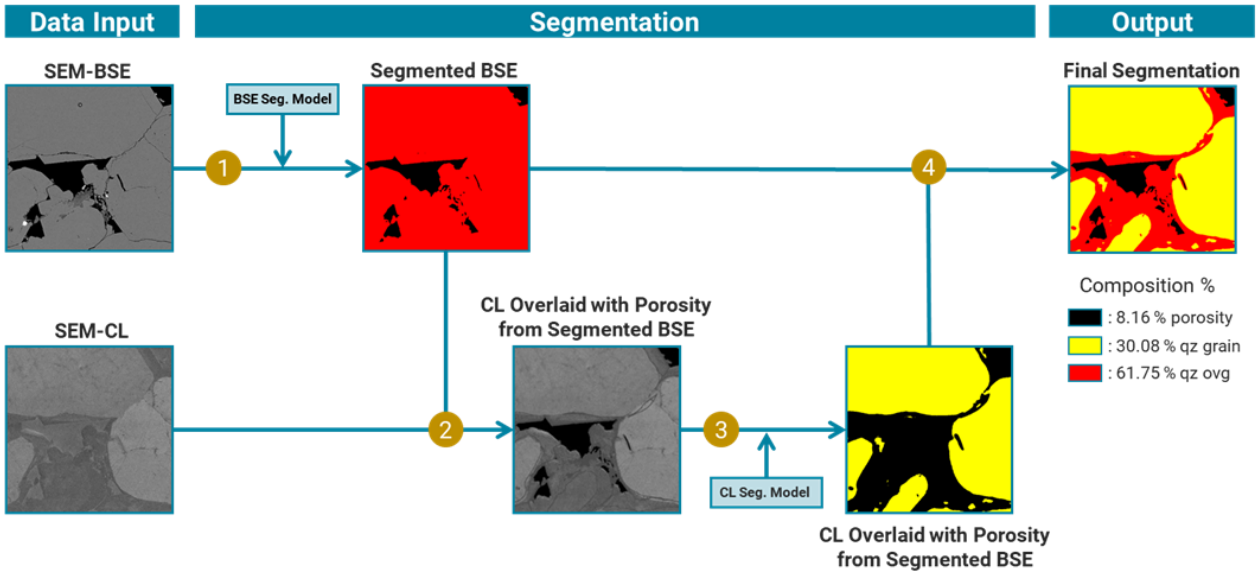

Figure 6: An illustration of automated segmentation workflow for quartz overgrowth detection using deep learning model.

6. RESULTS AND DISCUSSION

The evaluation of the U-Net segmentation model's performance entailed a comprehensive analysis over 50 epochs, involving metrics such as training and validation accuracy, loss, and the intersection over union (IoU) for each class. This process was conducted to assess the model's ability to generalize and learn from the data effectively. The accuracy and loss plots illustrate the model's progression, with training accuracy increasing and loss decreasing, signifying the model's improving aptitude in distinguishing and segmenting relevant features from the training data. The validation accuracy and loss offer insights into the model's performance on unseen data, ensuring that it is not merely memorizing the training data but rather learning patterns that are applicable to new data. The validation loss's variability points to the challenges the model faces with the complexity of the validation set. Additionally, observing the IoU for each class would provide a more granular understanding of the model's segmentation capability, as it directly measures the overlap between the predicted and ground truth segments, thus offering a precise metric for evaluating the quality of the segmentation across different classes within the dataset. This rigorous evaluation framework ensures that the model's predictive prowess is robust and not confined to the idiosyncrasies of the training set, thereby validating its deployment for practical segmentation tasks.

The U-Net segmentation model was evaluated over 50 epochs using various metrics such as training and validation accuracy, loss, and IoU. The model was tested for its ability to generalize and learn from data effectively. The accuracy and loss plots showed that the model improved in distinguishing and segmenting relevant features from the training data. The validation accuracy and loss ensured that the model was not just memorizing training data but learning patterns applicable to new data. The IoU for each class measured the overlap between predicted and ground truth segments, providing a precise metric for evaluating the segmentation quality across different classes. This rigorous evaluation validated the model's deployment for practical segmentation tasks.

6.1 BSE Segmentation Model Evaluation

The accuracy and loss plot (Fig. 7) of the BSE segmentation model reveals some interesting observations. Both training and validation accuracy experience a rapid increase during the initial epochs, indicating that the model is effectively learning from the data. This trend continues, with accuracy slightly increasing and plateauing at a high level of around 90%. Therefore, the model has successfully identified the classification necessary for BSE segmentation, namely pore space and quartz. However, there is a noticeable fluctuation in validation accuracy around epoch 37, which could be due to the model's response to the complexity of the validation data that it has not encountered during training. Nevertheless, the convergence of training and validation accuracy suggests that the model generalizes well and is not significantly overfitting.

As for the loss plot, it shows that the training and validation loss decrease as the number of epochs increases. The training loss (in yellow) starts with a steep decline at the beginning and then gradually decreases, ultimately leveling off as it approaches zero. This indicates that the model is efficiently minimizing the error on the training data. Meanwhile, the validation loss (in red) exhibits a similar pattern initially but shows more variability and a less steep decline, ultimately settling at a value higher than the training loss. This variability could indicate that the model is not performing consistently on the validation set, which is to be expected given the differences between training and validation datasets. However, throughout the training process, the close proximity of the training and validation loss lines indicates that the model maintains a good balance between learning from the training data and generalizing to new data. No significant overfitting is observed.

Based on the data presented in Table 1, the BSE Segmentation Model has a Mean IoU of 0.6008, indicating moderate performance. However, its IoU of 0.8627 for Pore Space is notably higher, suggesting high proficiency in detecting pore spaces within BSE images. The model excelled in segmenting Qz (quartz, including grain and overgrowth), achieving an IoU of 0.9398, which speaks to its excellent accuracy for this classification. These findings further support the model's ability to identify quartz and pore spaces in BSE images.

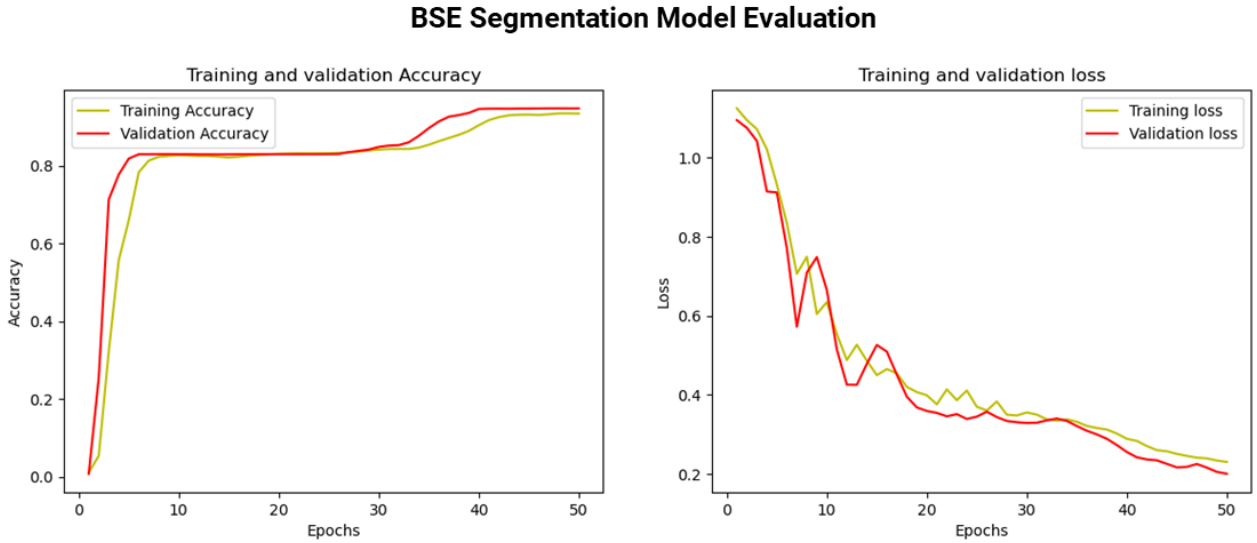

Figure 7: BSE segmentation model evaluation: performance in training and validation datasets.

6.2 CL Segmentation Model Evaluation

The accuracy plot in CL segmentation model (Figure 9) showed that both the training accuracy and the validation accuracy increased rapidly in the initial epochs. The training accuracy leveled off to slightly above 90% while the validation accuracy exhibited some fluctuations but generally remained stable after about 20 epochs. This close tracking of training and validation accuracy indicates that the model is generalizing well and not overfitting, which would have been evident if the training accuracy continued to increase while the validation accuracy began to decrease. On the other hand, the loss plot showed an initial sharp decrease in both the training loss and the validation loss. The training loss decreased to below 0.2, and the validation loss reduced to a similar range but with more volatility. The convergence of training and validation loss, particularly after about 30 epochs, with parallel trajectories suggests that the model is learning effectively and is stable as it does not exhibit the divergence that would suggest overfitting.

In summary, the analysis of the accuracy and loss plots suggests that the model has learned well from the training data and can generalize its predictions to unseen validation data effectively. Although the presence of noise in the validation lines, more in the loss graph than in the accuracy graph, is common in real-world scenarios, the overall trend indicates a successful training process with a model that is likely to perform well on new, unseen data.

The Mean IoU of the CL Segmentation Model is an impressive 0.9003, indicating exceptional overall segmentation performance. With an IoU of 0.8839, the model accurately predicts the *Qz Grain* class, and it is even more precise in identifying the *Non-Qz* Grain class with an IoU of 0.9168. *Non-Qz Grain* class remarkable accuracy can be attributed to the pore space value obtained from the BSE segmentation model that is overlaid on the CL image input before performing the CL segmentation. Consequently, the CL model can easily distinguish the *Non-Qz Grain* model by identifying only the quartz overgrowth part of the *Non-Qz Grain* segmentation since the pore space part has already been segmented.

In conclusion, the CL segmentation Model developed in this study demonstrates exceptional performance in segmenting crystal grains in CL images. The analysis of the accuracy and loss plots, as well as the Mean IoU values, showed that the model learned well from the training data and can generalize its predictions to unseen validation data effectively. Furthermore, with the integration of the BSE Segmentation Model, the CL model can accurately identify *Non-Qz* Grain class.

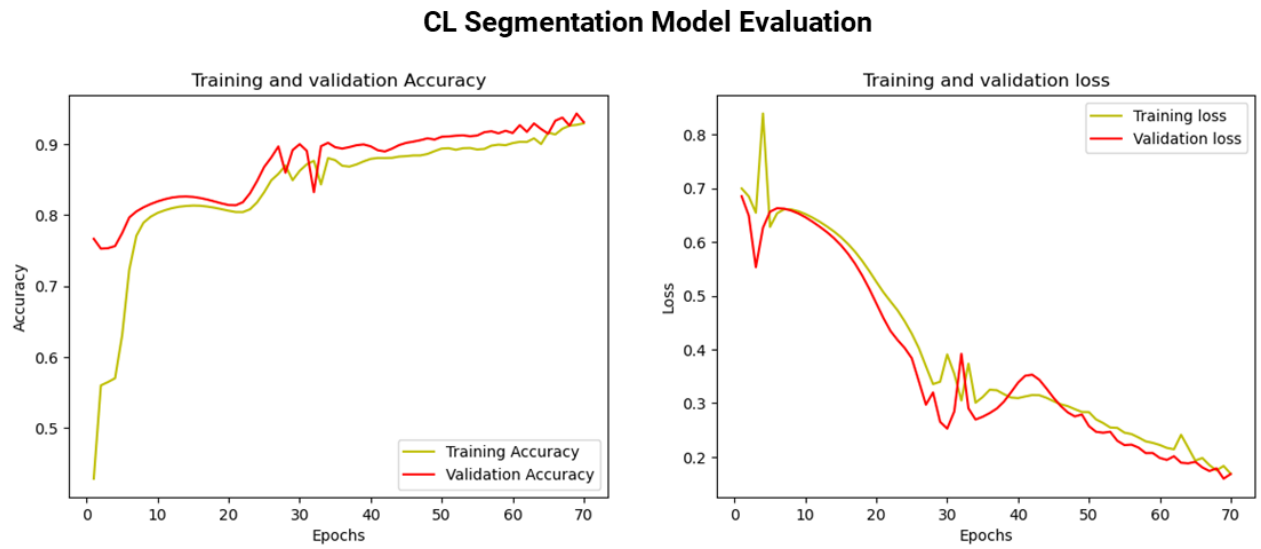

Figure 8: CL segmentation model evaluation: performance in training and validation datasets.

Table 1: Model evaluation for each of BSE segmentation and CL segmentation.

BSE Segmentation Model	CL Segmentation Model
Mean IoU: 0.6008	Mean IoU: 0.9003
IoU for Pore Space: 0.8627	IoU for Qz Grain: 0.8839
IoU for Qz (grain + ovg): 0.9398	IoU for Non Qz Grain: 0.9168
IoU for Other mineral: 0	

6.3. Segmentation Results

The efficacy of the U-Net algorithm in segmenting minerals in SEM images was rigorously tested using a variety of test images, as shown in Figure 9. The segmentation results reveal a nuanced performance of the U-Net model. In Images A and B, the algorithm demonstrates a high degree of accuracy, with the predicted segmentation closely aligning with the ground truth, indicating successful identification of the targeted mineral features without any significant issues.

Conversely, Images C and D present a more challenging scenario where the algorithm's performance wanes. Notably, the model struggles to accurately segment features around the periphery and in the finer structural details. The differentiation between quartz overgrowth and quartz grain proves particularly problematic, with the algorithm unable to reliably distinguish between the two in these specific instances. Additionally, the detection of other minerals, across all images, was not achieved, highlighting a limitation in the current model's capability. This suggests that the U-Net algorithm, while proficient in certain aspects of segmentation, still requires further refinement to improve its overall robustness and accuracy.

Overall, the U-net algorithm demonstrated competence in segmenting features from SEM images. However, its performance varied across different datasets, as evidenced by the inconsistent accuracy in some cases. This inconsistency points to the potential need for additional model training or optimization, possibly including the integration of more diverse training samples or the refinement of model parameters to account for the intricacies of SEM image data.

In summary, the U-Net algorithm has shown potential in automating the segmentation of SEM images for mineral detection, but the variability in its performance across different test cases implies that there is room for enhancement. This could involve fine-tuning the algorithm, expanding the training dataset, or incorporating additional feature recognition capabilities to improve the detection of a broader range of minerals, particularly in complex images where current performance is suboptimal.

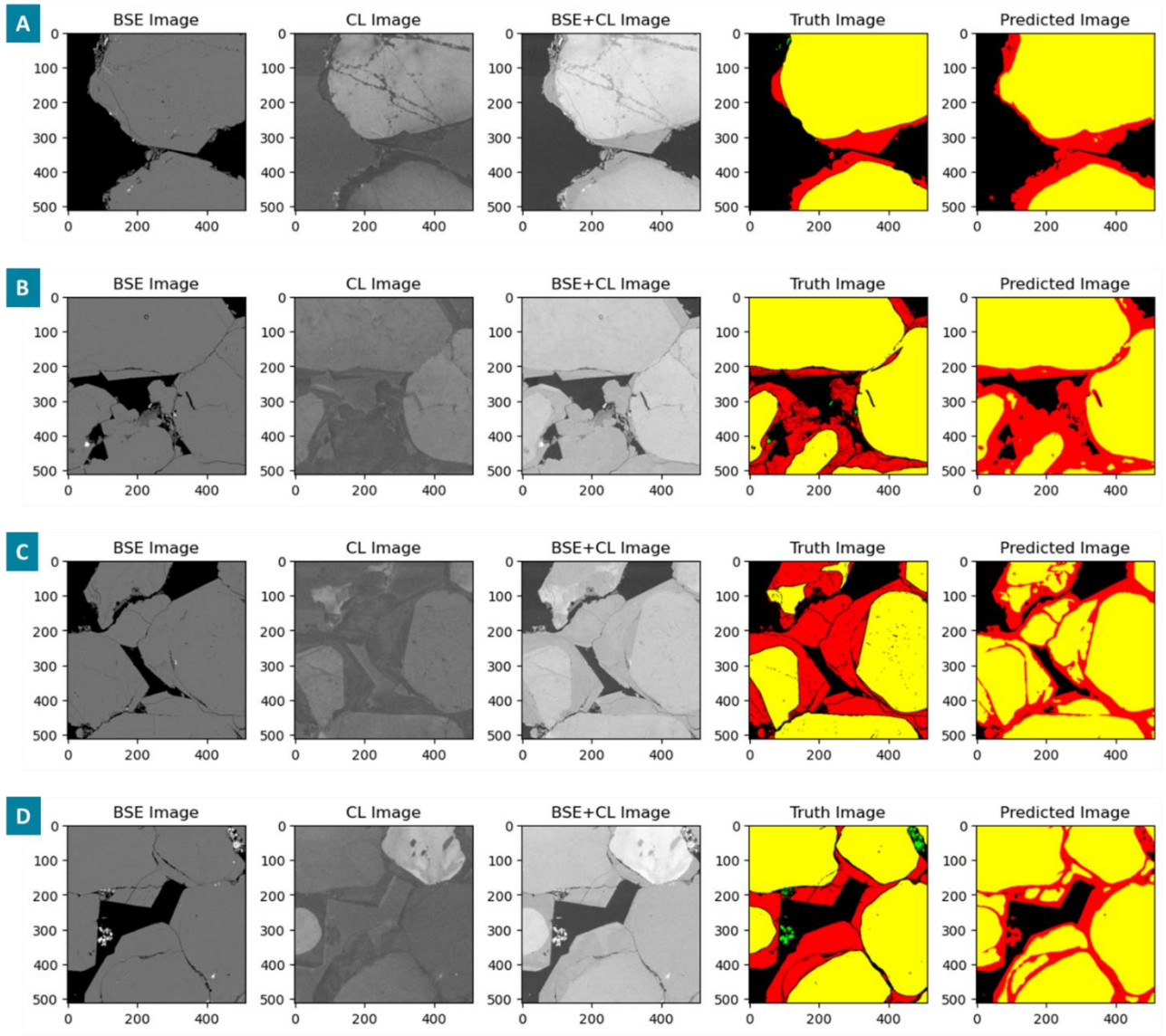

Figure 9: Results of final segmentation in four test set images and the corresponding original BSE, CL, and truth images. Black: porosity, red: quartz overgrowth, yellow: quartz grain.

6. CONCLUSION

This paper is a follow-up to the author's previous work, where a traditional machine learning algorithm (Random Forest) was utilized to perform mineralogy segmentation from SEM images - BSE and CL. The author explores the use of deep learning to enhance the segmentation process in this paper. The study implements a Convolutional Neural Network using the U-Net architecture, which successfully segments pore space, quartz overgrowth, and quartz grain in various image datasets. The segmentation of pore space and quartz (overgrowth and grain) was achieved through BSE images, while the segmentation of quartz grain boundary was performed using CL images. These were then combined to produce a final segmentation of the sample. The results demonstrate that the segmentation process is efficient in segmenting pore space, quartz overgrowth, and quartz grain.

However, the detection of quartz grain is still overestimated, despite the well-defined pore space segmentation. This is a common issue when the pixel intensity of the quartz grain in the CL image is similar to that of the quartz overgrowth. To solve this problem, the model needs to train on more datasets with similar pixel intensity between quartz grain and quartz overgrowth, and incorporating morphology detection principles into the algorithm could further improve its capability in delineating quartz grain. There is potential for future improvements in this regard.

Regarding future work, it may be beneficial for the author to explore a range of deep learning models and architectures. For instance, various architectures like Mask R-CNN and different types of deep learning models such as Generative Adversarial Networks (GANs) could be explored and compared to see which one is the most suitable for the research purpose. Furthermore, transfer learning could be

investigated as a means of fine-tuning a pre-trained model on a vast dataset to enhance the segmentation process. Lastly, developing a user-friendly, web-based tool for efficient and rapid segmentation of mineralogy samples could be considered for user convinence.

REFERENCES

Andaru, A., & Sausan, S. (2023). Intelligent Detection of SEM Mineralogy Using Dynamic Segmentation Algorithm in Geothermal Sedimentary Reservoir: Case Study with Quantification of Quartz Overgrowth. Society of Petroleum Engineers - SPE/IATMI Asia Pacific Oil and Gas Conference and Exhibition, APOG 2023. https://doi.org/10.2118/215327-MS

Bihani, A., Daigle, H., Santos, J. E., Landry, C., Prodanović, M., & Milliken, K. (2022). MudrockNet: Semantic segmentation of mudrock SEM images through deep learning. Computers and Geosciences, 158(October 2021). https://doi.org/10.1016/j.cageo.2021.104952

Knaup, A. S., Jernigen, J. D., Curtis, M. E., Sholeen, J. W., Borer, J. J., Sondergeld, C. H., & Rai, C. S. (2020). Unconventional reservoir microstructural analysis using SEM and machine learning. SPE/AAPG/SEG Unconventional Resources Technology Conference 2020, URTeC 2020, 3200–3212. https://doi.org/10.15530/urtec-2019-638

Latif, G., Bouchard, K., Maitre, J., Back, A., & Bédard, L. P. (2022). Deep-Learning-Based Automatic Mineral Grain Segmentation and Recognition. Minerals, 12(4), 455. https://doi.org/10.3390/min12040455

Liu, Y., Wang, X., Zhang, Z., & Deng, F. (2023). Deep learning in image segmentation for mineral production: A review. Computers and Geosciences, 180(May), 105455. https://doi.org/10.1016/j.cageo.2023.105455

Maitre, J., Bouchard, K., & Bédard, L. P. (2019). Mineral grains recognition using computer vision and machine learning. Computers and Geosciences, 130(February), 84–93. https://doi.org/10.1016/j.cageo.2019.05.009

Misra, S., Ganguly, E., & Wu, Y. (2019). Generalization of machine learning assisted segmentation of scanning electron microscopy images of organic-rich shales. In Machine Learning for Subsurface Characterization. Elsevier Inc. https://doi.org/10.1016/B978-0-12-817736-5.00011-9

Ronneberger, O., Fischer, P., & Brox, T. (2015). U-Net: Convolutional Networks for Biomedical Image Segmentation. In Medical Image Computing and Computer-Assisted Intervention – MICCAI 2015 (pp. 234–241). Springer International Publishing. https://doi.org/https://doi.org/10.1007/978-3-319-24574-4_28

Su, C., SHeng-jia, X., Zhu, K., & Zhang, X. (2020). Rock Classification in Petrographic Thin Section Images Based on Concatenated Concolutional Neural Networks. Earth Science Informatics, 9(4). https://doi.org/10.1007/s12145-020-00505-1

Tang, H., Wang, H., Wang, L., Cao, C., Nie, Y., & Liu, S. (2023). An Improved Mineral Image Recognition Method Based on Deep Learning. Jom, 75(7), 2590–2602. https://doi.org/10.1007/s11837-023-05792-9

Tian, X., & Daigle, H. (2019). Preferential mineral-microfracture association in intact and deformed shales detected by machine learning object detection. Journal of Natural Gas Science and Engineering, 63(January), 27–37. https://doi.org/10.1016/j.jngse.2019.01.003